



Potential of Celery (*Apium graveolens* L.) Essential Oil, against the corrosion of carbon steel in 1.0 M HCl: Electrochemical and quantum chemical study

A. EL Mostaphi¹, M. Larouj², H. Hartiti¹, M. Barrahi¹, M. Galai³,
M. EbnTouhami³, H. Oudda², M. Ouhssine¹

¹Laboratory of Agro-Physiology, Biotechnologies, Environment and Quality, Department of Biology, Faculty of Sciences, University Ibn Tofail, Kénitra, Morocco.

²Laboratory of Separation Processes, Faculty of Sciences, University Ibn Tofail, Kenitra, Morocco.

³Laboratory of Electrochemistry, the Corrosion and of Environment, University Ibn Tofail Kenitra, Morocco

Received 20 Dec 2018,
Revised 29 Jan 2019,
Accepted 21 Jan 2019

Keywords

- ✓ *Apium graveolens* L,
- ✓ Celery,
- ✓ Corrosion inhibition,
- ✓ HCl,
- ✓ Carbon steel,
- ✓ Density Functional Theory.

aminestare@hotmail.com
Phone: +212651433601

Abstract

Natural substances have been the subject of numerous researches in biology and chemistry to determine their potential biological and chemical activities. Their application as corrosion inhibitors is increasingly being seen as an important strategy. In the present work, we studied the effect of essential oil of *Apium graveolens*L. (Celery), which is recognized in the medical field by its analgesic, anti-inflammatory, and anti-bacterial among others; on corrosion of carbon steel C35 (CS) in a 1.0 M HCl environment using electrochemical and quantum chemical calculations techniques. With the objective of determining the most active component of its constituents and, which of them contributes most to the inhibition of corrosion, we conducted the extract from the oil of celery grains. The results obtained showed a very good improvement in the resistance of the CS in hydrochloric medium. We investigated the effect of certain parameters (concentration, temperature and immersion time) on celery inhibition efficiency. The results obtained show that the addition of celery to the aggressive solution slows down the corrosion process and that the inhibitory efficiency is increasing with the inhibitor concentration.

1. Introduction

Corrosion is the deterioration of a metal by an attack or a chemical reaction with its environment. It is a constant and continuous problem, often difficult to eliminate. Corrosion affects most industrial sectors and can cost billion dollars each year [1]. The use of the inhibitors to prevent the process of dissolution of metals remains an inevitable and very widespread strategy. The corrosion inhibitors are substances, which when they are added to weak concentrations in corrosive mediums, decrease or prevent the reaction of metal with its environment. An inhibitor can function by adsorption on metal surface thus involving the reduction speed corrosion by: (A) – an increase in the kinetics of the anodic and/or cathodic reaction, (b) - a fall the speed of diffusion of the reagents on the surface of metals, and (c) – a reduction in the electrical resistance of metal surface. What makes it possible to define the type of the inhibitor used (anodic, cathodic or mixed) [2].

Considerable efforts are made to find the compounds suitable to employ like corrosion inhibitors in various corrosive mediums in order to stop or to delay to the maximum the attack of a metal. Several works were completed on the nitro genized organic compounds and showed that these inhibitors have a good inhibiting effectiveness on various materials and in various corrosive mediums [3-4]. However, in some cases, these compounds present toxic effects on the organization and poison the environment [5]. Consequently, because as of environmental concerns, oils and the extracts of plants are regarded more and more as a source of green inhibitors of corrosion [6-7]. They are used for the protection of metals in the environment; in order to replace the toxic chemical products used currently [8].

The inhibition of the corrosion in 1.0 M HCl using celery essential oil extracts has been examined recently [8]. Such positive results inspired our team to examine the corrosion inhibition effect of celery belongs to Apiaceae family for steel in 1.0 M HCl medium. It is well known by its antioxidant properties and the modes containing these antioxidants can reduce the risk of the fungal diseases, diuretic, analgesic, anti-inflammatory drug, the detoxication, anti-bacteria antispasmodic, of the rules constraining, anti-contractions, of the convulsions, tonics of the stomach and carminative [9,10]. Electrochemical techniques such as potentiodynamic polarization and electrochemical impedance spectroscopy have been used to evaluate the corrosion inhibition process. The effect of the inhibitor concentration and temperature and immersion were carried out. Quantum chemical calculation based on the Density Functional Theory were conducted to study the electronic properties of inhibitor component.

2. Materials and Methods

2.1. Vegetal material and extraction

Equipment vegetable is made up by the grains wall and dry *Apium graveolens*.L. The fruits walls collected in the area of Marrakech in a movable, rich and wet ground in the following part are dried with the sun during approximately a week. Thus are dried with the drying oven at the weighed temperature of 40°C hanging two days then, is then ready for the extraction.

The system of hydro distillation clevenger is the equipment used during extraction of celery seeds (*Apium graveolens*.L). The steam which assembles balloon condenses in cool and changes in the form of droplets (water + oil) in one the 2nd time oil will be recovered at the end by a decantation by elimination of water and obtaining desired oil the extraction made continuously is of approximately three good fortunes.

2.2. Analysis chromatographic

Operating conditions of Gas chromatography (CPG): The chromatographic analysis of HE was carried out with a chromatograph in gas phase standard chromatograph in gas phase 7890b - agilent technologies the fragmentation is carried out by electronic impact with 70eV. The column used is a capillary tube HP 5MS (30mx0, 25mm). The thickness of the film is of 0,25µm. The temperature of the column is programmed of 50 with 250°C at a rate of 4°C.min⁻¹. The carrier gas is the helium whose flow is fixed at 1.5 mL.min⁻¹. The mode of injection is mode Split (report of escape: 1/70). The device is connected to a computer system managing a library of spectrum of mass NIST 98 and is controlled by software "HP ChemStation" making it possible to follow the evolution of the chromatographic analyses. The identification of the components was made on the basis of comparison between their indices of retention and those of the standard compounds of the computerized data bank (NIST 98). [4]

2.3. Material and aggressive solution

The steel used in this study is a carbon steel (carbon steel C35E and the American specification: SAE 1035) with a chemical composition (en% in weight) (0.370% of C) (0.230% If) (Mn 0.680%), (0.016% S) (0.077% Cr) (Ti 0.011%) (0.059% Ni) (Co 0.009%) (Cu 0.160%) and the iron rest (Fe). The samples of carbon steel were pretreated before the experiments by crushing with paper emery Sic (120 to 1200), then one rinses with distilled water, degreased in acetone in an immersion in a bath with ultrasounds during 5 min, one again washes them with water distilled and then dried with the room temperature before use. The acid solutions (HCl 1M) were prepared by dilution of an analytical quality of reagent HCl with 37% of water bi-distilled. The beach of celery concentration employed was 2-0, 5 (g/L) [11].

2.4. Electrochemical measurements

Electrochemical measurements were carried out using VoltaLab PGZ 100 controlled by ordinate associated with the software "Volta Master degree 4". The cell of corrosion used had three electrodes. The temperature was controlled by thermostat. The electrode of work is out of carbon steel with the surface of 1cm².

A calomel electrode saturated (SCE) was used as reference. All the potentials are given compared to this electrode. The counter-electrode is a plate of platinum of surface of 1 cm². Calomel electrode saturated was used as reference and an electrode out of platinum is used as counter-electrode. All the potentials are reported compared to SCE. All the electrochemical tests were carried out in solutions aired to 308 K.

For the curves of polarization, the working electrode is immersed in the test solution during 30 minutes until a steady state open circuit potential (E_{OCP}) was obtained. The scanning rate was of 1 mV/S starting from an initial potential of -900 mV to -100 mV (vs SCE). After the determination of the current to the stable condition with a given potential, the tension of sinusoidal wave (10 mV) peak with peak, at frequencies ranging between 100kHz and 10 MHz were superimposed on the potential of rest. Automatically controlled computer programs measures taken with the potential of rest after 30 min of exposure.. The diagrams of impedance are given in the representation of Nyquist. The best half-circle can be in form through the points of data in the diagram of Nyquist by using an adjustment of least squares non-linear to give the intersections with the x-axis [11].

2.5. Theoretical calculations

The quantum-based calculations were conducted using Gaussian program package, module version 9.0[12]. The calculations started without any geometry constraints until full geometry optimizations. The hybrid B3LYP functional level with a higher basis set denoted by 6-31G (d, p) of DFT has been used for the geometry optimization of the studied molecules[12–15]. The ionization energy and the electronic affinity were determined by the values of the energies of the HOMO and LUMO orbital[16]:

$$I = -E_{HOMO} \quad (1)$$

$$A = -E_{LUMO} \quad (2)$$

The values of I and A are exploited in order to find the values of the electro negativity and the global hardness of the inhibitory molecule[17]:

$$\chi = \frac{I+A}{2} \quad (3)$$

$$\eta = \frac{I-A}{2} \quad (4)$$

The fraction of electrons transferred (ΔN) from inhibitor to metallic surface was calculated using the equation[18]:

$$\Delta N = \frac{\phi - \chi_{inh}}{2(\eta_{Fe} + \eta_{inh})} \quad (5)$$

Where ϕ is the work function used as the appropriate measure of electronegativity of iron, and $\eta_{Fe} = 0$. The value of $\phi = 4.82$ eV for Fe (110) surface which is reported to have higher stabilization energy[17,18–20]. The local reactivity of inhibitor molecules (nucleophilic and electrophilic attacks) were obtained by condensed Fukui functions[21], using the following equations[22]:

$$f_k^+ = q_k(N + 1) - q_k(N) \quad (6)$$

$$f_k^- = q_k(N) - q_k(N - 1) \quad (7)$$

Where $q_k(N - 1)$, $q_k(N + 1)$, $q_k(N)$ are the charges of the cationic, anionic and neutral molecule, respectively.

3. Results and discussion

3.1. Chromatographic Analysis

The results of the analysis by Gas chromatography of the chemical composition of essential oil are presented in the **Table 1**, in which the identified compounds are listed according to the order of prevalence. Overall, 12 compounds were identified what corresponds to a percentage of 94.99% compared to the whole of the component isolated. D-Limonene seems the constituent majority one of the essential oil (79.15%), followed by Alpha-Hydroxypropylbenzene (4.23%), of the β -Selinene (9.25%), of Beta-Myrcene (1.93%). Biochemically speaking, this essential oil is primarily made up of a mono terpene (80%). Sesquiterpenes (4%). Lastly, the minority compounds belong to the family of oxides, aldehydes and alcohols sesquiterpenic (**Table 2**).

Table 1: Biochemical classes of the compounds identified in essential oil

Identification	Type of molecule	Chemical formula
Alpha-Thujene	Monoterpene	C ₁₀ H ₁₆
Beta-Pinene	Monoterpene	C ₁₀ H ₁₆
Bèta-Myrcene	Monoterpene	C ₁₀ H ₁₆
D-Limonène	Monoterpene	C ₁₀ H ₁₆
β -Selinene	Sesquiterpene	C ₁₅ H ₂₄
Caryophyllene oxide	Sesquiterpene	C ₁₅ H ₂₄

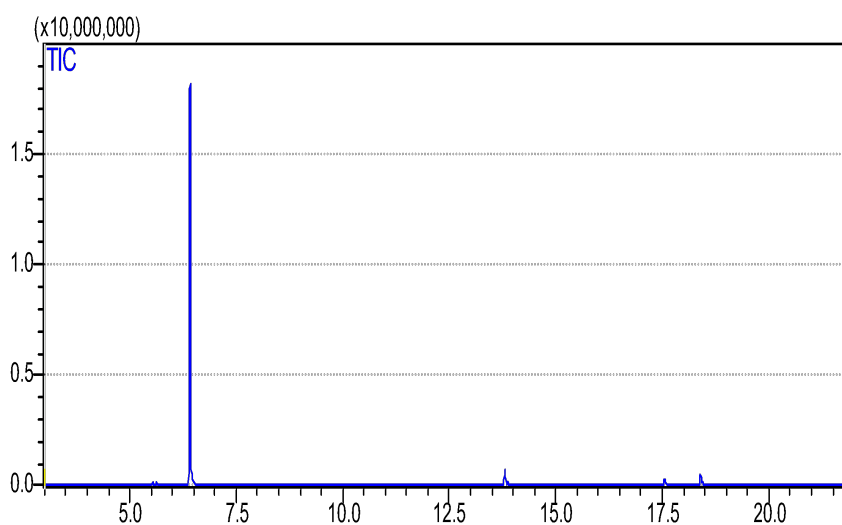


Figure 1: chromatogram for oil of the Apium graveolens.L

3.2. Effect of concentration

3.2.1. Curves of polarization

Cathodic and anodic curves of polarization of C35 steel, in absence and in the presence of various concentrations of Celery graveolensL. In 1.0 M HCl are presented in **figure 2**. Addition of the Celery moves the curves of polarization a slightly towards anodic potentials. Moreover, one can note that, the increase in the inhibitor concentration in the corrosive medium decreases the density of corrosion current, and that the total shape of the cathodic branches is unchanged. This indicates that the inhibitor does not change the cathodic process [25]. In the anodic process, it is observed that the

inhibitor effectively inhibits the steel corrosion up to -0.35 mV. In the higher potential, no inhibition effect can be observed. This is well known as desorption process of inhibitor molecules at higher anodic potential. Taken together, these results indicate that celery acts primarily like a mix-type inhibitor i.e. anodic and cathodic with an anodic predominance.

Table 2: Chemical composition of *Apium graveolens* L. essential oil

Identification	%
Alpha-Thujene	0.48
Hydroxybutric acid lactone	0.46
Beta-Pinene	1.04
Beta-Myrcene	1.93
D-Limonène	79.15
6-butyl-1,4-cycloheptadiène	0.64
Amyl benzene	0.96
β-Selinene	3.73
Caryophilene oxide	0.28
Beta-Selineol	0.33
2-chloro-1-(-2,4-dimethylphenyl)-2-methyl-1-propanone	1.76
Alpha-Hydroxypropylbenzene	4.23
Total of the percentages	95%

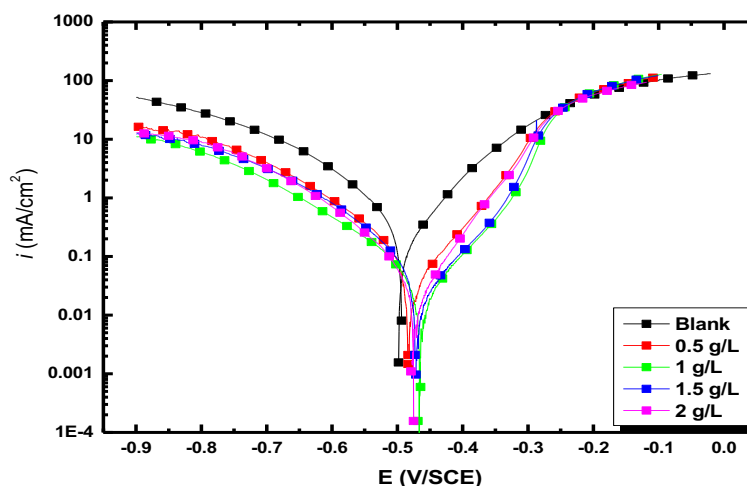


Figure 2: Polarization Curves of carbon steel in 1.0 M HCl in absence and presence of various concentrations of *Celery graveolens* L.

Table 3 lists the values of the electrochemical parameters derived from the curves of polarization such as the density of corrosion current (i_{corr}), the potential of corrosion (E_{corr}), the cathodic Tafel slope (β_c) [23], the anodic Tafel slope (β_a) as well as the inhibition efficiency (E%) which is defined by [24]:

$$E (\%) = \frac{i_{corr} - i_{corr}^*}{i_{corr}} \times 100 \quad (8)$$

Where i_{corr} and i_{corr}^* are the corrosion current density in the absence and presence of inhibitor respectively.

The results show that the corrosion current density i_{corr} decreases considerably with the increase in the celery concentration while no significant change can be observed in the corrosion potential E_{corr} values except a slight anodic displacement. Consequently, inhibition efficiency $E (\%)$ increased with the concentration of Celery to reach a maximum value of 96.66% at 1 g/L. From 2 g/L, the inhibitor effectiveness commences to decrease due to the less miscibility of celery in HCl solution.

Table 3: Electrochemical parameters of steel with various Celery concentrations in HCl 1M and the corresponding effectiveness of inhibition.

	E_{cor} (mV)	i_{corr} (mA /cm ²)	β_c (mV)	β_a (mV)	E%
Blank	-498	840	-105	99	-
0.5 g/L	-482	71	-95	74	91.54
1 g/L	-463	28	-94	76	96.66
1.5 g/L	-471	47	-93	77	94.40
2 g/L	-473	54	-86	60	93.57

3.2.2. The electrochemical impedance spectroscopy (EIS)

The purpose of the EIS diagrams is to get useful information into the mechanisms of corrosion and inhibition of carbon steel in 1.0 M HCl with inhibitor concentrations. The Nyquist diagrams of the steel immersed in 1.0 M HCl solution alone and in the presence of various Celery concentrations after 30 minutes of immersion are presented in **Figure 3**.

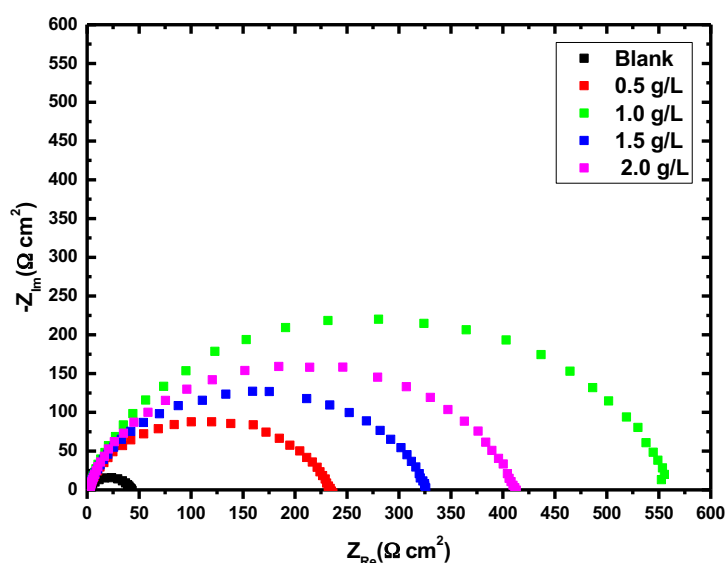


Figure 3: Diagrams of Nyquist obtained for steel in HCl 1M with various concentrations out of celery.

The values of the electrochemical parameters and the inhibition efficiency E(%) for various celery concentrations obtained are collected in **Table 4**. The inhibition efficiency is calculated according to the relation:

$$E (\%) = \left(\frac{R_t - R_t^*}{R_t} \right) \times 100 \quad (10)$$

Where R_t and R_t^* are respectively the values of the resistance of charge transfer of steel with and without addition of inhibitor. The values of the capacity of the double layer C_{dl} are obtained by the following relation [26]:

$$C_{dl} = \frac{1}{2\pi f_{max} R_t} \quad (11)$$

With C_{dl} is the capacity of the double-layer in ($\mu F cm^{-2}$), f_{max} is the maximum frequency (Hz) and R_t is the resistance of charge transfer ($k\Omega cm^2$) [27].

The diameters of the capacitive half-loops increase with the celery concentration, indicating that the inhibition efficiency is function of the concentration of the inhibitor. These graphs consist of only one capacitive boucle. This kind of diagram generally states that the reaction of corrosion is controlled by a process of transfer of charge on a solid electrode of heterogeneous and irregular surface. The general shape of the diagrams is very similar for all tests. This indicates that almost no change of the mechanism of corrosion occurred after the addition of inhibitor [28,29]. The values of the electrochemical parameters and the inhibition efficiency (E%) for various concentrations in inhibitor obtained by the EIS are presented in **Table 4**.

Table 4: Electrochemical parameters and effectiveness of inhibition of the corrosion of steel in HCl 1M without and with addition of various celery concentrations.

	R_t (Ωcm^2)	C_{dl} ($\mu F/cm^2$)	E%
Blank	40	294	-
0.5 g/L	231	108	83
1 g/L	558	89	93
1.5 g/L	325	97	87
2 g/L	414	91	90

From the results of impedance given in **Table 4**, we can observe that the values of the charge transfer resistance R_t increase with the increase in the celery concentration. This behavior is due to the adsorption of inhibitor molecules on the carbon steel surface [30]. In addition, an increase in the inhibition efficiency from 83% at 0.5g/L to 93% at 1 g/L was observed. The values of the capacity of the double-layer are also reduced in the presence of the inhibitor.

3.2.3. Adsorption studies

One of the proposed mechanisms of corrosion inhibition is the adsorption of inhibitor organic molecules on the metal surface by the replacement of already adsorbed water molecules forming a compact barrier film thus blocking active sites of corrosion as represented in the equation:



The process of adsorption can be evaluated by fitting the surface coverage θ as a function of concentration at constant temperature to obtain various adsorption isotherms like Langmuir, Freundlich, Temkin *etc.* and the best fit with almost unit correlation constant was selected. In the present investigation, the best-fit isotherm was found to be Langmuir, which is represented by the equation [31]:

$$\frac{C}{\theta} = \frac{1}{K_{ads}} + C \quad (12)$$

Where θ is the surface coverage, K_{ads} is the adsorption-desorption equilibrium constant, C is the concentration of inhibitor.

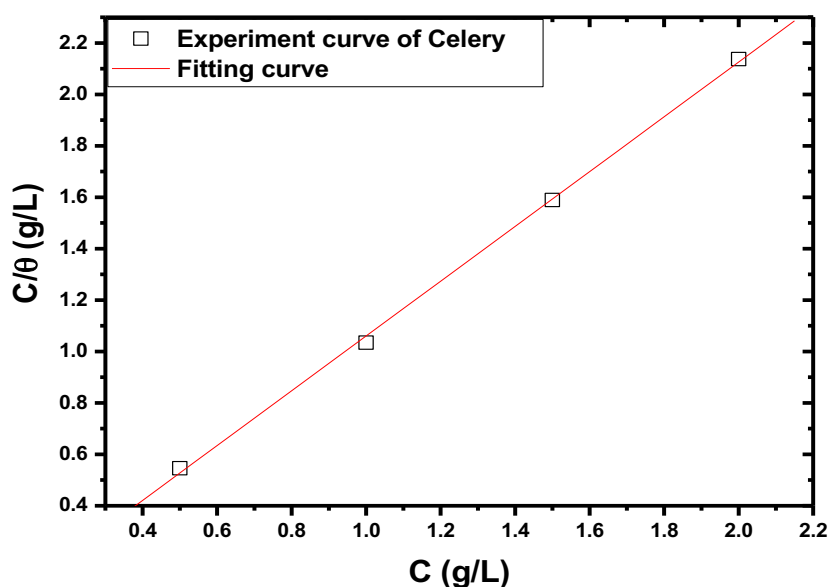


Figure 4: Langmuir isotherm of Celery obtained by using surface coverage values calculated from the Nyquist plots

The adsorption-desorption equilibrium constant (K_{ads}) which measures the strength of adsorption was given by the reciprocal of slope. The free energy of adsorption ΔG_{ads}° is correlated to (K_{ads}) as [32]:

$$\Delta G_{ads}^{\circ} = -RT \ln(55.5 \times K_{ads}) \quad (13)$$

where R is universal gas constant in kJ mol/L, 55.5 is taken as concentration of water in mol/L and T is the temperature.

The ΔG_{ads}° values gave insight into the type of adsorption like physisorption, chemisorption or mixed. The adsorption parameters calculated are listed in **Figure 4**. The high value of adsorption constant indicates the stronger adsorption. The negative value of ΔG_{ads}° reflected the spontaneous and stable adsorption of Celery on mild steel surface [33].

3.2.3 Kinetic and thermodynamic studies

Temperature is an important factor which influences the process of corrosion and modifies the adsorption of inhibitor on metal surface. Various complex changes like rapid etching, desorption of inhibitor, decomposition of inhibitor etc. occur on the metal surface on the inhibited acid-metal solution during temperature enhancement. The influence of the temperature on the effectiveness of Celery inhibition was also studied by the potentiodynamic polarization. The curves of polarization obtained in 1.0 M HCl with and without addition of 2g/L of Celery during one hour of immersion in the range of temperature (298-328K) are presented in **Figures 5** and **6**.

Figure 6 show that the temperature has a great effect on the inhibitor's effectiveness. The corrosion current density value of steel without inhibitor increases considerably at higher temperatures while the inhibitor still effective in the studied temperature range. The electrochemical parameters obtained by exploitation of the Tafel lines are listed in **Table 5**.

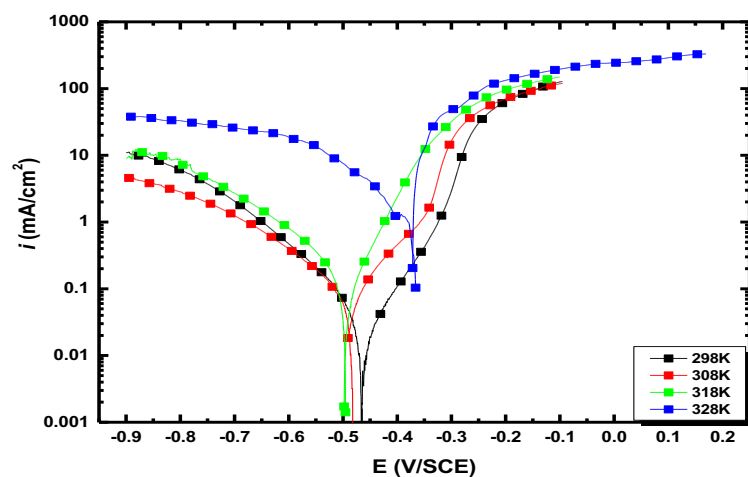


Figure 5: Curves of polarization of steel in 1.0 M HCl in absence and in the presence of 2g/L of celery at various temperatures.

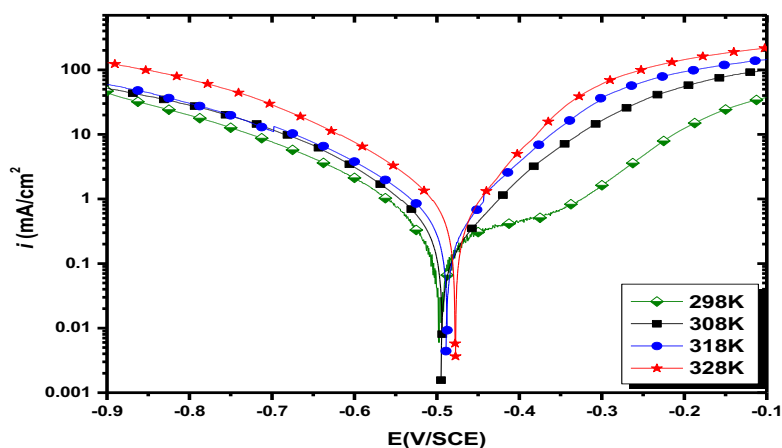


Figure 6: Potentiodynamic polarization curves of carbon steel in 1.0 M HCl at various temperatures.

Table 5: electrochemical parameters of the steel of different Temperature involved and absence from celery in HCl 1M.

		$E_{corr}(mV)$	$I_{corr}(\mu A/cm^2)$	$B_c (mV)$	$B_a(mV)$	$E (%)$
298	Inhibitor	-463	28	-94	76	96.67
	Blanc	-498	840	-92	203	-
308	Inhibitor	-481	50	-119	70	96.87
	Blanc	-491	1600	-178	200	-
318	Inhibitor	-494	107	-110	60	95.58
	Blanc	-475	2420	-165	191	-
328	Inhibitor	-390	450	-119	74	85.48
	Blanc	-465	3100	-151	170	-

It is apparent from results in the **Table 5** that the value of the (i_{corr}) increases on increasing temperature for uninhibited as well as inhibited solutions. It is also clearly seen that inhibition efficiency is almost stable with increasing of the temperature, which is an indication of the high adsorption of tested inhibitor at highest temperatures. The increased value of i_{corr} is attributed to the

less desorption of the Celery's inhibitor molecules from mild steel surface at elevated temperatures. These results confirm that celery inhibits corrosion in the interval of temperature studied [34].

The Arrhenius and Transition state equations were used for studying the activation parameters, the apparent activation energy E_a^* for metal dissolution in 1.0 M HCl in the absence and presence of inhibitor were determined using Arrhenius equation [35]:

$$I_{corr} = k \exp\left(\frac{-E_a^*}{RT}\right) \quad (14)$$

Where R, the universal gas constant and k, the Arrhenius pre-exponential factor. **Figure 7** represents the Arrhenius plots of $\ln(i_{corr})$ against $1/T$ for the corrosion of mild steel in 1.0 M HCl solution in the absence and presence of Celery at concentration (1 to 2 g/L of inhibitor).

The E_a^* values of the inhibited and inhibitor free solutions were obtained from the slopes of the Arrhenius plot and are tabulated in **Table 6**. The activation parameters like enthalpy of activation, ΔH_a^* and the entropy of activation, ΔS_a^* for the corrosion of mild steel in acidic medium were obtained by transition state equation [36]:

$$I_{corr} = \frac{RT}{Nh} \exp\left(\frac{\Delta S_a^*}{R}\right) \exp\left(-\frac{\Delta H_a^*}{RT}\right) \quad (15)$$

Where N is the Avogadro's number, h is Planck's constant, ΔS_a^* is the entropy of activation and ΔH_a^* is the enthalpy of activation. A plot of $\ln(I_{corr}/T)$ vs $1/T$ produces a straight line **Figure 8** with a slope of $(\Delta H_a^*/R)$ and an intercept of $(\ln(R/N.h) + (\Delta S_a^*/R))$ from which the activation parameters ΔH_a^* and ΔS_a^* were calculated and presented in **Table 6**. It could be seen from the table that E_a values increases by the introduction of inhibitor into the corrosive solution.

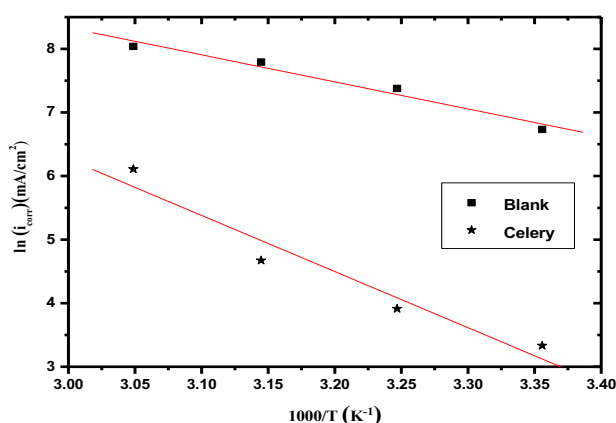


Figure 7: Arrhenius plots for carbon steel corrosion in 1.0 M HCl solution containing various concentrations of Celery.

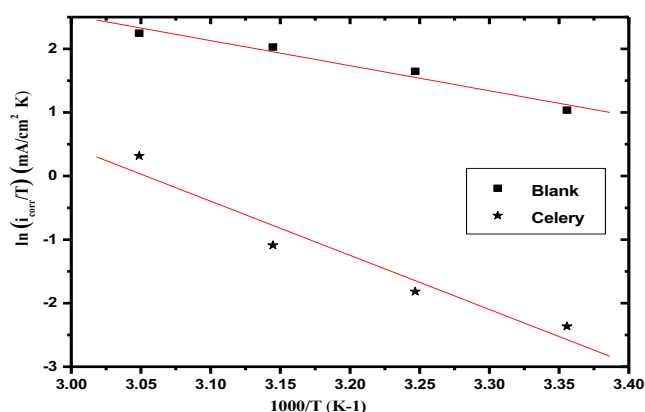


Figure 8: Transition state plots of $\ln i_{corr}/T$ versus $1000/T$ for the corrosion of carbon steel in 1.0 M HCl solution containing various concentrations of Celery

Table 6: The value of activation parameters for mild steel in 1.0M HCl in the absence and presence of Celery at different temperatures.

Inhibitor	E_a (kJ/mol)	ΔH_a (kJ/mol)	ΔS_a (J/mol)	$E_a - \Delta H_a$ (kJ/mol)
Blank	35.38	32.78	-76.86	2.6
Celery	73.39	70.79	18.64	2.6

It can be inferred that in the presence of inhibitor, the acid ions must cross higher threshold energy to get collide with the metal molecules and to cause corrosion compared to that in an inhibitor free solution [37].

The condition of $E_a(\text{inh}) > E_a(\text{Blank})$ is consistent for the process of adsorption of inhibitor on most active adsorption sites having lowest energy and the corrosion takes place chiefly on the higher energy active sites [38].

The increase in activation energy is consistent with the reported trends in literature and this type of behavior is associated with preferable physical adsorption [39]. It can be inferred from the trend of activation energy that corrosion rate of mild steel is mainly controlled by activation parameters. The positive values of enthalpy of activation point towards the endothermic nature of metal dissolution process. The increase in ΔH_a^* in the presence of inhibitor than that in its absence may be attributed to the deceleration of metal dissolution by the inhibitor molecules [40].

The value of entropy of activation is found to be higher and positive in the inhibited solution compared to the negative value in the inhibitor free solution. This reflects the decrease in randomness on converting from reactants to activated complex due to the adsorption of organic inhibitors from the acid solution, which could be regarded as a quasi substitution process between the organic inhibitor in the aqueous phase and water molecules at the electrode surface.

3.3. Quantum chemical calculations of the limonene inhibitor molecule

In order to investigate the relationship between inhibition efficiency and molecular reactivity at microscopic level, and to further explain the mechanism of inhibition based on molecular structural parameters, quantum chemical calculations were carried out on the studied inhibitor. **Figure 9** shows the fully optimized geometries, HOMO called as the highest occupied molecular orbital, LUMO called as the lowest unoccupied molecular orbital. The reactive sites of the molecules can be better studied by analyzing the HOMO and LUMO while the reactivity trend can be identified by studying the electronic parameters [41]. The HOMO and LUMO electron density of Limonene are localized almost on the entire molecular structure showing the tendency of the mentioned compound towards chemical and physical interactions, which further support the experimental investigations.

Table 7 reports the quantum chemical parameters, i.e. HOMO and LUMO energies, HOMO-LUMO gaps ($\Delta E = E_{\text{HOMO}} - E_{\text{LUMO}}$) and fraction of electron transferred ΔN .

In the most cases, the chemical stability of the molecule can be deduced from the energy gap (ΔE), where a smaller ΔE might confirm that the molecule is much easier to be polarized and adsorbed on the metal surface [42]. If $\Delta N > 0$, it exhibits the electron transfer from the molecule to the metal surface and if $\Delta N < 0$, the electron transfer from metal surface to the molecule [43,44].

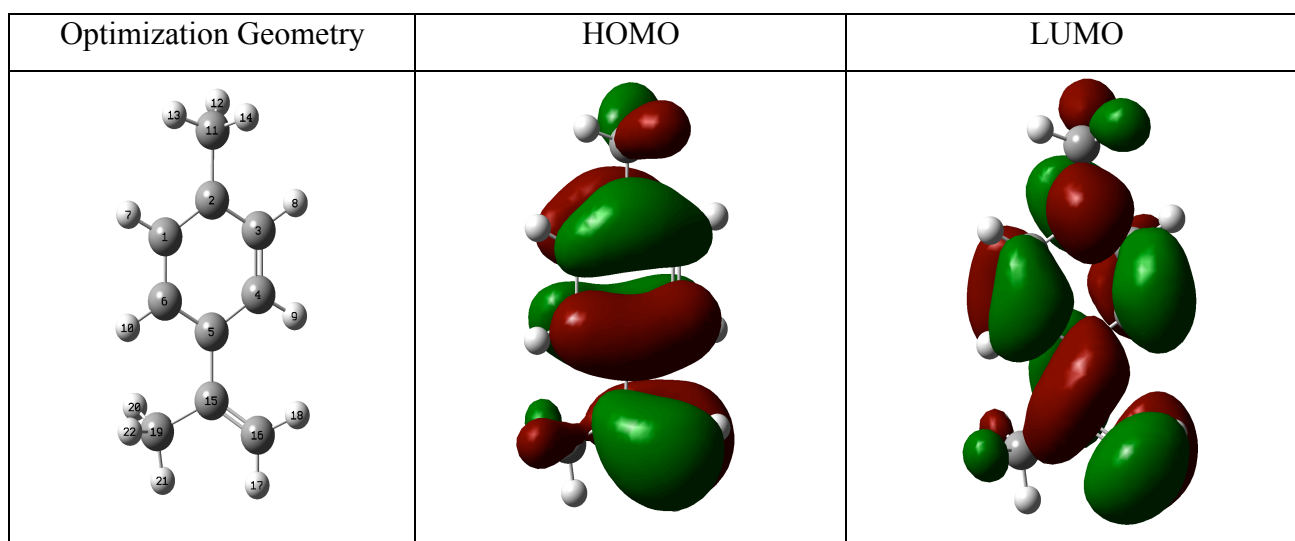


Figure 9: Optimized molecular structure, HOMO and LUMO orbital of limonene calculated at DFT/6-31G(d, p)

Table 7 : The computed quantum chemical parameters for limonene compound.

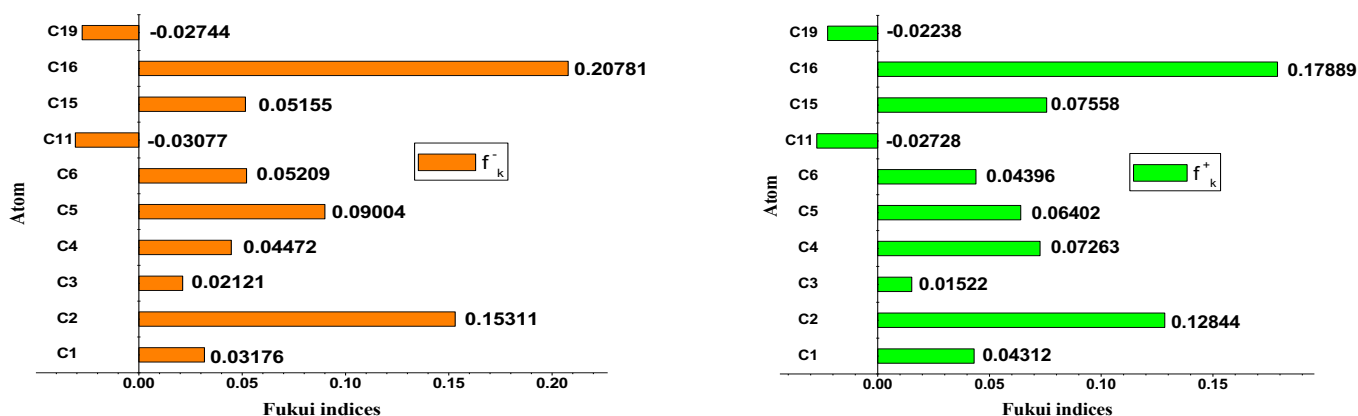
Quantum Parameters	μ Debye	E_{HOMO} (eV)	E_{LUMO} (eV)	ΔE_{gap} (eV)	ΔN_{110}
limonene	0.5467	-5.8472	-0.5437	5.3035	0.3063

In order to obtain additional information about the donor-acceptor interactions, the Fukui function (FF) calculations are one of the useful means for this purpose **Table 8**. The local reactivity indices also define the most reactive regions in a molecule [45]. The nucleophilic and electrophilic behaviour of different sites of the inhibitor molecule are mainly determined by the maximum threshold f_k^- and f_k^+ values. When a molecule accepts electrons the changes in electron density are measured by the f_k^+ values while the f_k^- values give the measures of the changes in electron density when the electrons are lost by the molecules [46].

So, for limonene, the favorable centers for electron acceptance i.e., nucleophilic attacks are C(2), C(4), C(15) and C(16) atoms having f_k^+ values 0.128, 0.073, 0.076 and 0.179 respectively. Moreover, the susceptible sites for electrophilic attacks i.e., electron donation are C (2), C(5) and C (16) atoms having f_k^- values 0.153, 0.090, and 0.208 respectively. Further, both of the electron density distribution in the HOMO and LUMO of the studied molecule and Fukui indices signify the same reactive sites for the corresponding donor-acceptor type interaction on the metallic surfaces **Figure 10** [46].

Table 8: Fukui functions of limonene calculated at B3LYP/6-31G(d, p).

Atom	f_k^-	f_k^+
C1	0.032	0.043
C2	0.153	0.128
C3	0.021	0.015
C4	0.045	0.073
C5	0.090	0.064
C6	0.052	0.044
C11	-0.031	-0.027
C15	0.052	0.076
C16	0.208	0.179
C19	-0.027	-0.022

**Figure 10**: Graphical representation of the calculated Fukui indices of Limonene

Conclusion

The essential oil of *Apium graveolens*.L (Celery) ensures the inhibition of steel C35 corrosion in 1 M HCl medium by formation of a protective film and the adsorption of Celery obeys to Langmuir isotherm model. The polarization study shows that the Celery acts as a mixed type inhibitor, while the electrochemical impedance spectroscopy results show that as the inhibitor concentration is increased, the charge transfers resistance rise and the double layer capacity decreases. The tests concerning the effect of the temperature were carried in the interval (298K - 328K), this test showed that the increase in the temperature affects the inhibiting Celery power. Indeed, the effectiveness of the inhibitor which was from 90.8% to 25 °C becomes 62.9% to 35 °C. The DFT simulation supports the good inhibition performance of Celery.

References

1. M.H. Hussin, M. Kassim, *Mat. Chem. Phys.* 125 (2011) 461.
2. A. Ostovari, S.M. Hoseinie, M. Peikari, S.R. Shadizadeh, S.J. Hashemi, *Corros. Sci.* 51 (2009) 1935.
3. A. Elouafi, B. Hammouti, H. Oudda, S. Kertit, R. Touzani, A. Ramdani, *Anti Corros. Meth. Mater.* 49 (2002) 199.
4. M. Tourabi, K.Nohair, A. Nyassi, B. Hammouti, A. Chetouani, F. Bentiss, *J. Mor. Chem.* 1 (2013) 33.
5. N.O. Eddy, E.E. Ebenso, *Pure Appl. Chem.* 2 (2008) 46.
6. A.F. Gualdrón, E.N. Becerra, D.Y. Peña, J.C. Gutiérrez, H.Q. Becerra, *J. Mater. Environ. Sci.* 4 (2013) 143.
7. N. Lotfi, H. Lgaz, M. Belkhaouda, M. Larouj, R. Salghi, S. Jodeh, H. Oudda, B. Hammouti, *J. Arab. Chem. Envir. Res.* 1 (2014) 13.
8. E. Chaieb, A. Bouyanzer, B. Hammouti, M. Benkaddour, *Appl. Surf. Sci.* 246 (2005) 199.
9. S. Fujisawa, T. Atsumi, Y. Kadoma, H. Sakagami, *Toxicology* 177 (2002) 39.
10. L.W. Wadell, H.N. Crooks, P.L.Carmichael, *Toxicological Sci.* 79 (2004) 38.
11. J.J. Macheix, A. Fleuriot, J.A. Billot, *Fruit phenolics* (CRC Press Inc., Boca Raton, 1990).
12. Mj. Frisch, G. Trucks, Hb. Schlegel, G. Scuseria, M. Robb, J. Cheeseman, J. Montgomery Jr, T. Vreven, K. Kudin, Jc. Burant, Gaussian 03, revision c. 02; Gaussian, Inc Wallingford CT. 4 (2004).
13. A.D. Becke. *J. Chem. Phys.* 84 (1986) 4524.
14. A.D. Becke. *J. Chem. Phys.* 98 (1993) 5648.
15. C. Lee, W. Yang, R.G. Parr, *Phys. Rev. B.* 37 (1988) 785.
16. M.J. Dewar, W. Thiel, *J. Am. Chem. Soc.* 99 (1977) 4899.
17. R.G. Pearson, *Coord. Chem. Rev.* 100 (1990) 403.
18. S. Martinez, *Mater. Chem. Phys.* 77 (2003) 97.
19. R.G. Pearson, *J. Org. Chem.* 54 (1989) 1423.
20. R.G. Pearson, *Inorg. Chem.* 27 (1988) 734.
21. A. Kokalj, *Chem. Phys.* 393 (2012) 1.
22. R.G. Parr, W. Yang, *J. Am. Chem. Soc.* 106 (1984) 4049.
23. R.R. Contreras, P. Fuentealba, M. Galván, P. Pérez, *Chem. Phys. Lett.* 304 (1999) 405.
24. K. Anupama, K. Shainy, A. Joseph, *J. Bio- Tribo-Corros.* 2 (2016) 2.
25. M. Dupart, F. Dabosi, F. Moran, S. Rocher, *Corrosion NACE*, 37 (1981) 262.
26. A. Bonnel, F. Dabosi, C. Deslouis, M. Duprat, M. Keddou, B. Tribollet, *J. Electrochem. Soc.* 130 (1983) 753.
27. A. Harmaoui, H. Bourazmi, M. El Fal, M. Boudalia, M. Tabyaoui, A. Guenbour, A. Bellaouchou, Y. Ramli, E. M. Essassi. *J. Mater. Environ. Sci.* 6 (2015) 2509.
28. A. Popova, E. Sokolova, S. Raicheva, M. Christov, *Corros. Sci.* 45(2003)33.
29. H. Keleş, S.Akça, *Arab. J. Chem.* 12 (2019) 236-248

30. A. Yurt, A. Balaban, S. UstÄun Kandemir, G. Bereket, B. Erk, *Mater. Chem. Phys.* 85 (2004) 420
31. X. Li, S. Deng, H.Fu, *Prog. Org. Coat.* 67 (2010) 420.
32. M. Faustin, A. Maciuk, P. Salvin, C. Roos, M. Lebrini, *Corros. Sci.* 92 (2015) 287.
33. I.B. Obot, N.O. Obi-Egbedi, *Curr. Appl. Phys.* 11 (2011) 382.
34. A. Doner, R. Solmaz, M. Ozcan, G. Kardas, *Corros. Sci.* 53 (2011) 2902.
35. I.A. Ammar, F.M. El Khorafi, *Werkst. Korros.* 24 (1973) 702.
36. M. Messali , M. Larouj , H. Lgaz , N. Rezki, F.F. Al-Blewi , M.R. Aouad, A. Chaouiki , R. Salghi, Ill-Min Chung *Journal of Molecular Structure* 1168 (2018) 39.
37. Ekemini Ituen, Abosede Jamesc, Onyewuchi Akaranta, *Portugaliae Electrochim. Acta* 34 (6) (2016) 417.
38. A. Khadiri, A. Ousslim, K. Bekkouche, A. Aounit, A. Elidrissi, B. Hammouti, *Portugaliae Electrochim. Acta* 32 (1) (2014) 35.
39. A. Bousskri, R. Salghi, Anejjar, M. Messali, S. Jodeh, O. Benali, M. Larouj, I.Warad, O. Hamedc, B. Hammouti, *Portugaliae Electrochim. Acta* 34 (1) (2016)1.
40. R. Geethanjali, S. Subhashini, *Portugaliae Electrochim. Acta* 33 (2015) 35.
41. Hassane Lgaz, Ill-Min Chung, Mustafa R. Albayati, Abdelkarim Chaouiki, Rachid Salghi, Shaaban K. Mohamed *Arabian Journal of Chemistry* (2018). <https://doi.org/10.1016/j.arabjc.2018.08.004>
42. M. Yadav, S. Kumar, I. Bahadur, D. Ramjugernath. *Int J Electrochem Sci.* 9 (2014) 3928.
43. A. Kokalj. *Electrochim. Acta* 56 (2010) 745.
44. N. Kova_cevi_c, A. Kokalj. *Corrosion Sci.* 53 (2011) 909.
45. H. Lgaz, R. Salghi, Subrahmanya Bhat, K., Chaouiki, A., Shubhalaxmi, Jodeh, S. *J. Mol. Liq.* 244 (2017) 154.
46. H. Lgaz, Subrahmanya Bhat, K., Salghi, R., Shubhalaxmi, Jodeh, S., Algarra, M., Hammouti, B., Ali, I.H., Essamri, A. *J. Mol. Liq.* 238 (2017) 71.

(2018) ; <http://www.jmaterenvirosci.com>